

# A bilayer vascular scaffold with spatially controlled release of growth factors to enhance *in situ* rapid endothelialization and smooth muscle regeneration

Yuanfei Wang<sup>a</sup>, Tong Wu<sup>b,\*</sup>, Jialing Zhang<sup>d</sup>, Zhendong Feng<sup>b</sup>, Meng Yin<sup>e,\*</sup>, Xiumei Mo<sup>c,\*</sup>

<sup>a</sup> Qingdao Stomatological Hospital Affiliated to Qingdao University, Qingdao 266001, China

<sup>b</sup> Institute of Neuroregeneration and Neurorehabilitation, Qingdao University, Qingdao 266071, China

<sup>c</sup> State Key Lab for Modification of Chemical Fibers and Polymer Materials, College of Chemistry, Chemical Engineering and Biotechnology, Donghua University, Shanghai 201620, China

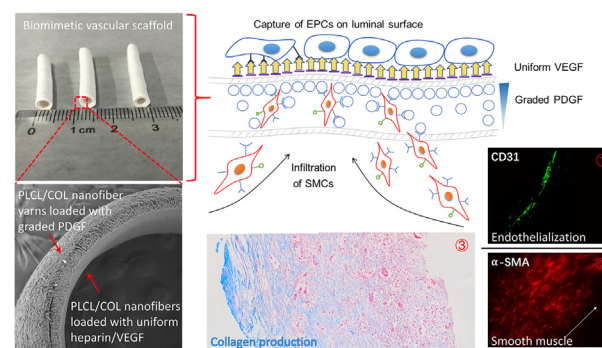
<sup>d</sup> Department of Cardiovascular Center, Children's Hospital of Fudan University, Shanghai 201102, China

<sup>e</sup> Department of Cardiothoracic Surgery, Shanghai Children's Medical Center, Shanghai Jiaotong University School of Medicine, Shanghai 200127, China

## HIGHLIGHTS

- A bilayer vascular scaffold was designed with both topographic cues and biological guidance.
- Vascular endothelial growth factors and platelet derived growth factors were controlled for release.
- The recruited smooth muscle cells were organized with circumferential alignment.
- *In-situ* rapid endothelialization, smooth muscle remodeling, and collagen-rich ECM production were all observed.

## GRAPHICAL ABSTRACT



## ARTICLE INFO

### Article history:

Received 23 October 2020

Received in revised form 16 February 2021

Accepted 5 March 2021

Available online 10 March 2021

### Keywords:

Electrospun nanofibers

Controlled release

Endothelialization

Smooth muscle cell infiltration

Circumferential alignment

## ABSTRACT

When transplanting a scaffold to repair defected vascular tissues, there is a critical need to achieve *in-situ* rapid endothelialization together with the circumferential alignment and ingrowth of smooth muscle cells. To this end, we hereby design and fabricate a bilayer vascular scaffold with spatially controlled release of growth factors. The lumen of such a scaffold was made of electrospun poly(L-lactide-co-caprolactone) and collagen (PLCL/COL) nanofibers loaded with uniform heparin and vascular endothelial growth factors (VEGF), while its outer layer was composed of circumferentially aligned, PLCL/COL nanofiber yarns loaded with graded platelet derived growth factors (PDGF) increasing from the outermost toward the interior of the scaffold. With the controlled release of VEGF and PDGF from the scaffold, we showed a continuous greater release percentage (*ca.* 15%) of VEGF relative to PDGF over a duration of almost one month *in vitro*. At two-month post implantation in a rat abdominal aorta defect model, we observed rapid endothelialization at the luminal surface and orientated smooth muscles infiltrating inside the vascular wall. In particular, loose connective tissues rich in collagen fibers were produced at the outermost layer of the vascular scaffold, indicating the capability of such kind of vascular scaffold for *in-situ* vascular repair or regeneration.

© 2021 The Author(s). Published by Elsevier Ltd. This is an open access article under the CC BY-NC-ND license (<http://creativecommons.org/licenses/by-nc-nd/4.0/>).

## 1. Introduction

It has been documented that two important microenvironments (*i.e.*, circulating blood and surrounding tissues) determine lumen

\* Corresponding authors.

E-mail addresses: [twu@qdu.edu.cn](mailto:twu@qdu.edu.cn) (T. Wu), [yinmengmdphd@163.com](mailto:yinmengmdphd@163.com) (M. Yin), [xmm@dhu.edu.cn](mailto:xmm@dhu.edu.cn) (X. Mo).

anticoagulation, endothelium formation, smooth muscle cell infiltration, and neotissue formation during the repair of an injured blood vessel after *in-situ* implanting a vascular scaffold [1,2]. Among others, lumen patency is the prerequisite for an implanted vascular scaffold to remain effective in repairing the defected tissues [3]. In this regard, a rich variety of vascular scaffolds have been developed to inhibit the formation of thrombus and/or promote the development of an endothelial layer at the luminal surface. For example, a great number of previous studies have shown heparin, a clinically-used anticoagulation agent, has effective impact on luminal anticoagulation of a vascular scaffold [4–8]. For the purpose of long-term anticoagulation, however, a more effective way is to accelerate the formation of endothelium on the luminal surface of the vascular scaffold by capturing and proliferating endothelial progenitor cells (EPCs) and endothelial cells (ECs) in the bloodstream [9–11]. In one study, West-Livingston et al. has shown the conjugation of bioactive antibodies such as EC-specific antibodies (CD31), vascular endothelial cadherin, vascular endothelial growth factor receptor 2, and von Willebrand factor onto electrospun vascular scaffolds made of a blend of PCL and collagen for *in-situ* rapid endothelialization [9]. In another typical example, Wang et al. modified electrospun PCL vascular scaffolds with vascular endothelial growth factor (VEGF) and heparin through repeated electrostatic adsorption self-assembly [12]. In this case, they realized an early and full release of VEGF to promote rapid endothelialization, followed by a gradual but sustained release of heparin to keep long-term patency. VEGF has also been incorporated into electrospun nanofibers to induced EPC differentiation and reendothelialization [13].

Despite of the progress in accelerating the regeneration of endothelial tissues, a pending challenge is the synergistic regulation between *in-situ* endothelialization at luminal surface and the regeneration of smooth muscles surrounding the vascular wall when designing a tubular scaffold [14]. One should expect a vascular scaffold to form confluent and mature endothelium as soon as possible to inhibit thrombus formation and subsequent production of oriented smooth muscles to provide sufficient support to maintain the vascular structure [15,16]. To this end, a wide range of multilayered, tubular scaffolds have been designed for the regeneration of vascular tissues [17–20]. Among others, multilayered scaffolds made of electrospun nanofibers have emerged as a promising class of alternatives in the recent decade [17,20–22]. In a typical example, Wen et al. developed a tri-layered vascular scaffold containing microRNA-126 and microRNA-145, respectively, in the inner and middle layers of an electrospun nanofiber scaffold [17]. The microRNA-126 was incorporated to accelerate the synthesis of VEGF and fibroblast growth factors, while the microRNA-145 played a role in modulating the contractile phenotype of SMCs. Such a scaffold showed accelerated endothelialization, improved regeneration of contractile smooth muscle cells (SMCs), and promoted production of normal extracellular matrix (ECM). In another example, cellularized vascular construct with autologous EPCs-derived ECs and SMCs were fabricated using electrospun nanofibers of a blend of poly( $\epsilon$ -caprolactone) and collagen, which showed sustained structural integrity with confluent and mature EC and SMC layers in the scaffold [22]. However, there is still remaining a major incentive in promoting the circumferential orientation together with the infiltration of SMCs inside the vascular wall.

Here we designed a bilayer vascular scaffold with two continuous layers to accelerate endothelialization and promote the circumferential alignment and penetration of SMCs. Through the manipulation of topographic cues provided by electrospun nanofibers and nanofiber yarns, we were able to induce the formation of dense endothelial layer on the nanofibrous luminal surface, along with the circumferential alignment and infiltration of SMCs inside the outer layer consisting of the nanofiber yarns (Scheme 1). In particular, we incorporated heparin and VEGF into the nanofibers of the inner layer of the vascular scaffold to enable early patency and the rapid proliferation of EPCs. By offering a biological cue using graded platelet derived growth factor (PDGF)

increasing from the outmost layer toward the interior of the vascular scaffold, the SMCs are capable of growing and penetrating inside the vascular wall through the chemotaxis effect. Taken together, we focus on the recapitulation of the multiple layers of native blood vessels together with the synergistically controlled release of VEGF and PDGF to facilitate the tissue regeneration. Post *in-situ* implantation in a rat abdominal aorta defect model, we investigated the preliminary performance of the vascular scaffold in terms of rapid endothelialization and the regeneration of smooth muscles.

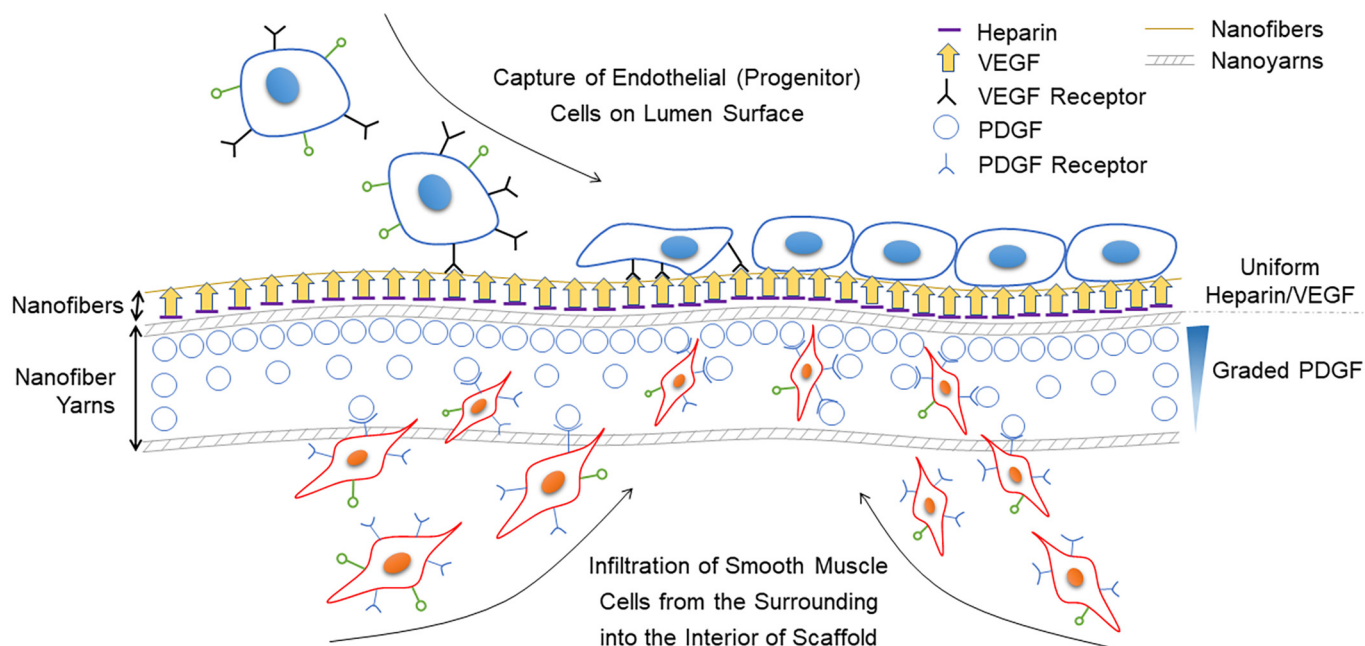
## 2. Experimental section

### 2.1. Preparation of the bilayer vascular scaffold

The inner layer of the vascular scaffold was fabricated *via* coaxial electrospinning. Poly(L-lactide-co-caprolactone) (PLCL, 50:50, Mn: 450000, Jinan Daigang Biomaterial Co., Ltd.) and porcine-derived type I collagen (COL, Mn: 100000, Chengdu Kele Bio-tech Co., Ltd.) were blended at a weight ratio of 3:1, and then dissolved in 1,1,1,3,3,3-hexafluoro-2-propanol (HFIP) at a total concentration of 10 wt% (shell solution). 0.15 g/mL heparin (Shanghai Rich Joint Co., Ltd.) and 20  $\mu$ g/mL vascular endothelial growth factor (VEGF, Sigma-Aldrich) were dissolved in 1 mg/mL bovine serum albumin/ phosphate-buffered saline (BSA/PBS) solution and used as the core solution. A high voltage (DC) of 14 kV and flow rates at 1.0 mL/h (shell) and 0.1 mL/h (core) were applied to obtain the PLCL/COL nanofibers loaded with heparin and VEGF (PLCL/COL-Hep/VEGF). A rotating rod (500 rpm, 2-mm diameter, and 10-cm length) was used as the collector. At 2 h post electrospinning, the PLCL/COL nanofiber yarns loaded with a gradient of PDGF (PLCL/COL-PDGF) were electrospun and sequentially collected as the outer layer of the vascular scaffold. The nanofiber yarns were fabricated using a modified bi-directional conjugated electrospinning setup integrated with coaxial electrospinning. Briefly, PLCL/COL solution was electrospun on the right side, while 10 wt% PLCL/COL (3:1, w/w) and 20  $\mu$ g/mL PDGF dissolved in 1 mg/mL BSA/PBS solution were separately used as the shell and core solution for electrospinning on the left side. The flow rate of PLCL/COL on the right side was fixed as 1.0 mL/h. On the left side, the flow rates of PLCL/COL and PDGF were changed in the sequence of 1.0/0 to 2.0/0.4, 1.0/0.2, 1.0/0.1, and 1.0/0 mL/h, and kept for 10, 90, 90, 60, 10 min, respectively. The vascular scaffold was crosslinked by the vapor generated from 25% aqueous glutaraldehyde (GA) solution for 30 min and then stored in a vacuum oven.

### 2.2. Characterization

We took the photograph of the as-obtained vascular scaffold using a digital camera (Nikon D5600). The microstructure of the vascular scaffold was imaged using a scanning electron microscope (SEM, JSM-5600, Japan) at an accelerating voltage of 15 kV and a working distance of 8 mm. The core-shell structure of one individual PLCL/COL-Hep/VEGF and PLCL/COL-PDGF fiber was also observed by a transmission electron microscope (HT7700, Hitachi). The mechanical property of the vascular scaffold and its inner and outer layers were investigated by a universal material testing machine (H5K-S, Hounsfield, UK) with a 50 N load cell under the condition of 20 °C, a relative humidity of 65%, and an extension rate of 10 mm/min. The compliance of the vascular scaffold was measured and calculated using the TM 1 Test Bench System (Bose Electro force, USA) with a fluid flow rate of 100 mL/min and a testing frequency of 1 Hz as we previously described [23]. The release behavior of the payloads was investigated by placing the vascular scaffold (50 mg) in 5 mL PBS solution and incubated in a continuous horizontal shaker (120 rpm) under the condition of 37 °C. At each time point (1, 3, 5, 8, 12, 16, 20, 25, 30, 35, and 45 days), 1 mL solution was pipetted for investigation and 1 mL of fresh PBS solution was supplemented. The release amount of heparin was determined by the Toluidine blue method,



**Scheme 1.** Schematic illustration showing the capture of EPCs on lumen surface and the infiltration of SMCs with the use of a bilayer vascular scaffold for *in-situ* vascular tissue regeneration. The release of heparin could inhibit the formation of thrombus at the early-to-mid stage post grafting. While the homogeneously released VEGF can accelerate endothelialization, the graded release of PDGF is able to promote the infiltration of SMCs from the surrounding microenvironment toward the interior of the scaffold.

while that of VEGF and PDGF was measured using the corresponding ELISA kit (Sigma-Aldrich). The cumulative release profiles of heparin, VEGF, and PDGF were plotted, respectively.

### 2.3. *In vitro* cell culturing

We investigated the growth behavior of EPCs and smooth muscle cells (SMCs) on the inner and outer layers of the vascular scaffold, respectively. The EPCs were reanimated and cultured using an EGM-2 MV Bullet kit (Lonza, Switzerland) supplemented by 10% fetal bovine serum (FBS) and 1% antibiotic—antimycotic under the condition of 5% CO<sub>2</sub> and 37 °C. The PLCL/COL-Hep/VEGF nanofibers were used for investigation, together with the PLCL/COL-Hep and PLCL/COL nanofibers serving as control groups. The EPCs were seeded on the different types of nanofibers with a density of  $2.0 \times 10^4$  cells per well after disinfecting the nanofibers by 75% ethanol vapor, and the proliferation of EPCs at 1, 4, and 7-day post culturing was measured using a Cell Counting Kit-8 (Dojindo Lab., Japan). The morphology of the EPCs after culturing for 4 days were imaged by SEM and an inverted fluorescence microscope (Olympus IX71, Japan), respectively. Briefly, the samples were fixed by 4% paraformaldehyde solution at 4 °C for 4 h, and then treated by dehydration using gradient concentrations of ethanol for SEM observation. For the fluorescent imaging, the fixed samples were permeabilized using 0.1% Triton X-100 (Sigma, USA) for 5 min at room temperature, followed by staining by rhodamine-conjugated phalloidin (Invitrogen, USA). Between each step, the samples were rinsed twice by PBS solution.

To investigate the morphology and infiltration of SMCs, we cultured SMCs on PLCL/COL nanofibers (NF), PLCL/COL nanofibers loaded with graded PDGF (NF-P), PLCL/COL nanofiber yarns (NFY), and PLCL/COL nanofiber yarns loaded with graded PDGF (NFY-P) for 4 days, respectively, in Dulbecco's modified Eagle's medium (DMEM) with 10% fetal bovine serum and 1% antibiotic—antimycotic under the condition of 5% CO<sub>2</sub> and 37 °C. Then, the samples were stained by rhodamine-conjugated phalloidin and used for fluorescent imaging to show the cell morphology. To compare the infiltration of SMCs on the different types of samples, we fixed the samples with 4% paraformaldehyde

solution at 4 °C for 4 h, embedded them in freezing medium and froze at −80 °C, followed by sectioning the samples into slices with a thickness of 10 μm. Then, the slices were treated by hematoxylin and eosin (H&E) staining following the standard protocol and imaged using an optical micrograph.

### 2.4. *In vivo* evaluation

We conducted a primary study to show the performance of the vascular scaffold for *in-situ* vascular tissue regeneration. All of the *in-vivo* experiments were completed following the institutional guidelines of animal care and with the permission of Animal Ethics Committee of Shanghai Children's Medical Center, Shanghai Jiaotong University School of Medicine (Shanghai, China). Eight male SD rats with average weight of 300 g were used to construct the abdominal aorta replacement models with a 10-mm defect section. The as-obtained vascular scaffolds with 2 mm in diameter and 12 mm in length were used for *in-situ* implantation. At two-month post implantation, the rats were euthanized to harvest the scaffolds for investigation. The explanted samples were fixed using 4% paraformaldehyde and incubated at 4 °C for 4 h, followed by paraffin embedding and sectioning to several 10-μm thick slices. Half slices were used for H&E and Masson's trichrome staining following the standard protocols, while the rest slices were stained by CD31 and α-SMA primary antibodies to examine the regeneration of endothelium at luminal surface and smooth muscle regrowth inside the vascular wall. 4',6-Diamidino-2-phenylindole dihydrochloride was used to stain the nuclei of cells. Two rats were used as the control groups (the autologous vessels) for the same staining.

### 2.5. Statistical study

All the results are presented as mean ± standard deviation with at least three parallel measurements. Statistical analysis was made using Student's *t*-test. Differences were considered statistically significant when  $P < 0.05$ .

### 3. Results and discussion

#### 3.1. Fabrication and characterization of the bilayer vascular scaffold

We fabricated the bilayer vascular scaffold by sequentially depositing the Hep/VEGF-encapsulated, PLCL/collagen (PLCL/COL-Hep/VEGF) nanofibers and the PLCL/collagen nanofiber yarns loaded with a gradient of PDGF (PLCL/COL-PDGF) on a rotating stainless-steel rod with a diameter of 2 mm (Fig. 1). As shown by the schematic illustration in Fig. 1A, the PLCL/COL-Hep/VEGF nanofibers were fabricated by coaxial electrospinning, which was used to fabricate a wide range of payload-incorporated nanofibers [24]. In this case, Hep/VEGF was dissolved in an aqueous solution containing bovine serum albumin (BSA) as the core, and PLCL/COL was served as the shell. To fabricate the PLCL/COL nanofiber yarns loaded with graded PDGF increasing from the outmost to the interior of the scaffold, a modified setup integrating coaxial with conjugated electrospinning was utilized. On the right side of the conjugated electrospinning setup, PLCL/COL solution was used for electrospinning. While on the left side, a coaxial electrospinning setup

**Table 1**

Ultimate stress and elongation of the vascular scaffold versus porcine coronary artery.

Samples	Ultimate Stress (MPa)	Elongation
Inner layer	13.4 ± 1.9	145.7 ± 14.1%
Outer layer-parallel	17.5 ± 2.0	198.9 ± 20.2%
Outer layer-perpendicular	1.6 ± 0.3	208.6 ± 18.7%
Vascular scaffold-parallel	14.9 ± 2.4	219.6 ± 17.8%
Vascular scaffold-perpendicular	3.7 ± 0.6	302.3 ± 11.1%
Porcine coronary artery	2.6	100%

was employed with PDGF dissolved in the BSA solution as the core and PLCL/COL as the shell. During this electrospinning process, the flow rates regarding PLCL/COL and PDGF were tuned in the sequence of 1.0/0 to 2.0/0.4, 1.0/0.2, 1.0/0.1, and 1.0/0 mL/h, and kept for 10, 90, 90, 60, 10 min, respectively. The two thin layers consisting of the nanofiber yarns without PDGF (*i.e.*, 1.0/0 mL/h for 10 min) were designed as barriers to slow down the release of PDGF to the lumen fluid and the surroundings.

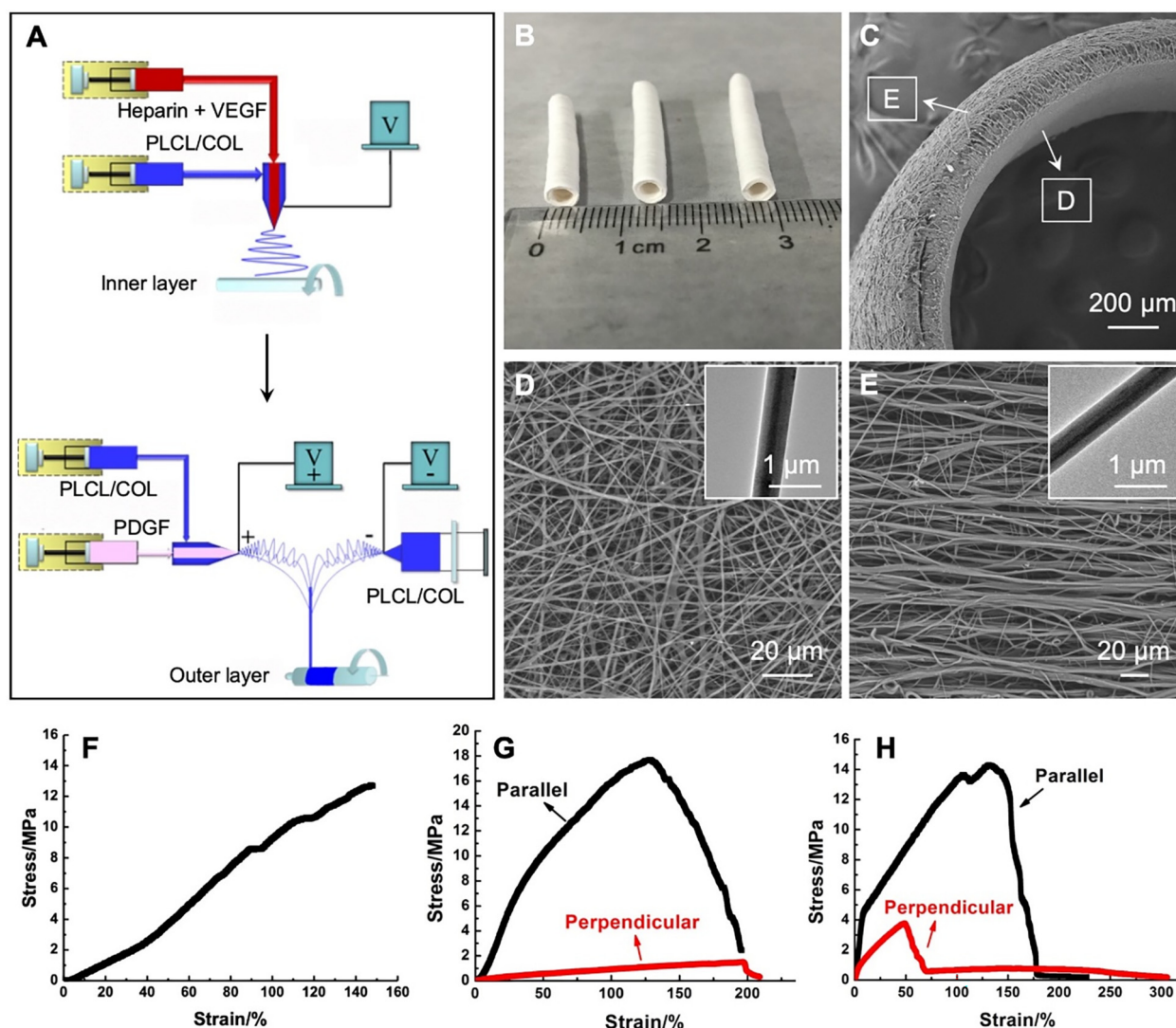


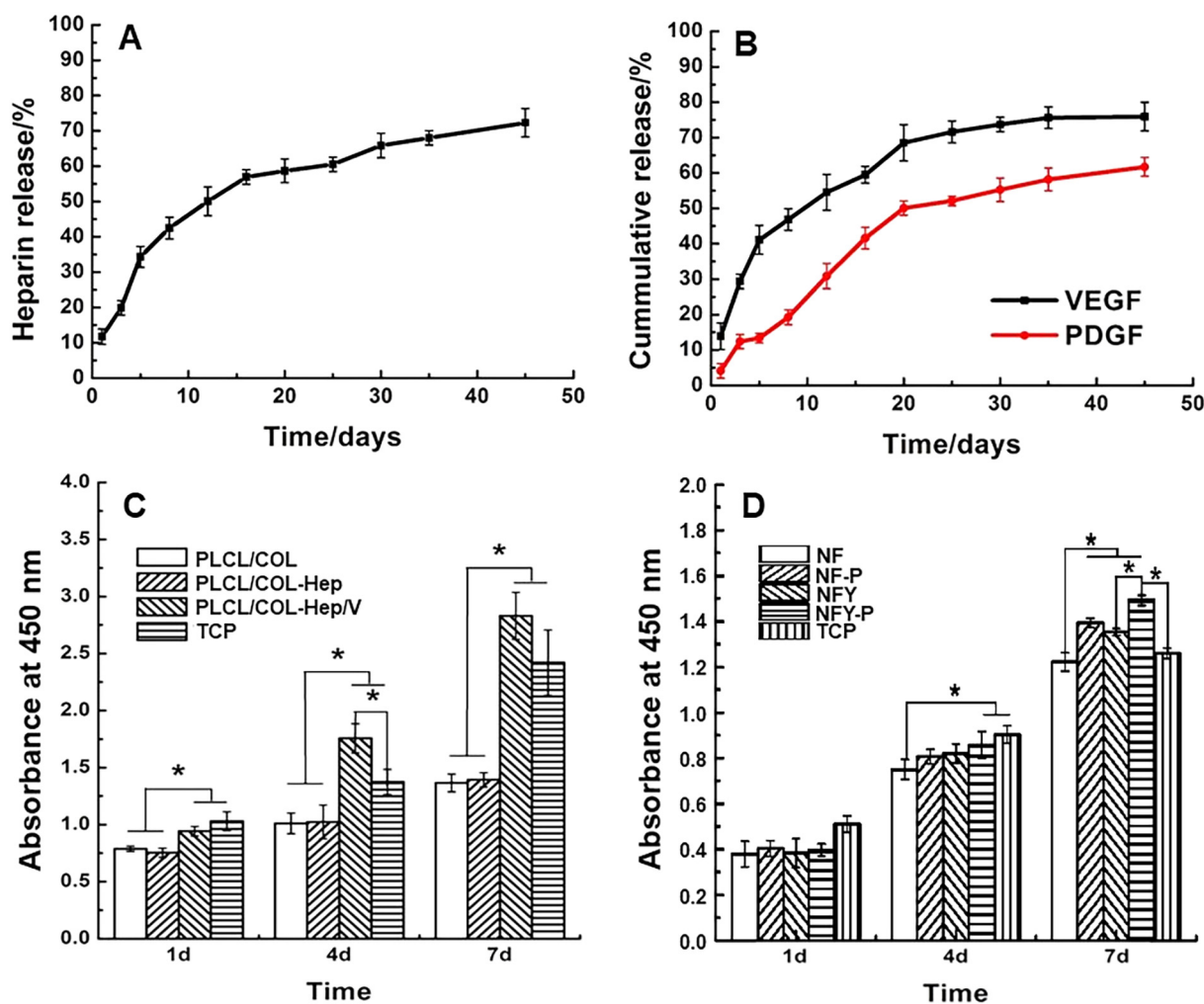
**Fig. 1.** (A) Schematic illustration showing the fabrication of the bilayer vascular scaffold through the integration of coaxial electrospinning and conjugated electrospinning. (B) Photograph showing the vascular scaffold with an inner diameter of 2 mm and a thickness of 1 mm. (C – E) SEM images showing (C) the cross section of the vascular scaffold, (D) the PLCL/COL-Hep/VEGF nanofibers and (E) PLCL/COL-PDGF nanofiber yarns electrospun using flow rates of 0.1 mL/h for core solution and 1 mL/h for shell solution. The inserts in (D) and (E) are TEM images separately showing the core-shell structure of one individual PLCL/COL nanofiber loaded with (D)Hep/VEGF and (E) PDGF in the core. (F – H) Representative stress-strain curves showing the tensile mechanical properties of the (F) inner layer made of PLCL/COL-Hep/VEGF nanofibers, (G) outer layer made of PLCL/COL-PDGF nanofiber yarns, and (H) the bilayer vascular scaffold.

**Table 2**  
Compliance of the vascular scaffold versus human saphenous vein and e-PTFE.

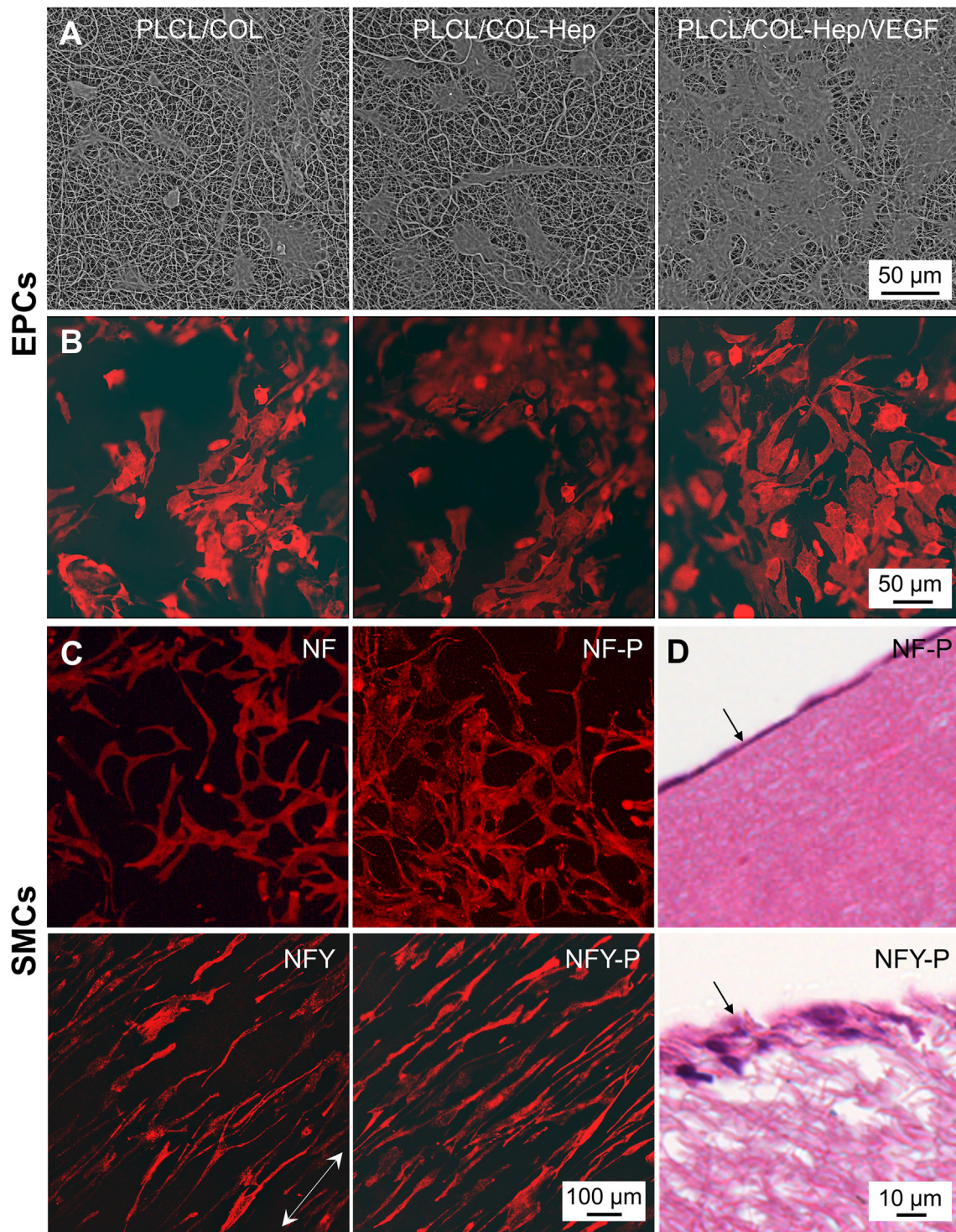
Samples	Compliance %/100 mmHg
Vascular scaffold	1.33 ± 0.05
Human saphenous vein	0.7–1.5
e-PTFE	0.1

Fig. 1B shows a digital photograph of the as-obtained vascular scaffold after removal of the collecting rod. The scanning electron microscopy (SEM) images in Fig. 1, C – E show the cross-sectional structure of the vascular scaffold and the surface morphologies of the inner and outer layer, respectively. The inner layer composed of dense PLCL/COL-Hep/VEGF nanofibers with an average diameter of  $551 \pm 95.3$  nm was designed to avoid the leakage of blood, inhibit thrombus, and accelerate the endothelialization. On the other hand, the circumferentially aligned, PLCL/COL-PDGF nanofiber yarns with an average diameter of  $7.9 \pm 2.2$  μm were used to tune the orientation and induce the infiltration of SMCs from the surroundings toward the interior of the scaffold. The insets in Fig. 1, D and E show the typical transmission electron microscopy (TEM) images of one individual fiber of PLCL/COL loaded with Hep/VEGF and PDGF, respectively. The core-shell structures clearly demonstrate the incorporation of growth factors in the fibers.

We then investigated the mechanical property of the vascular scaffold (Fig. 1, F – H and Table 1). The ultimate mechanical strength and the elongation at break of the inner layer made of PLCL/COL-Hep/VEGF nanofibers were  $13.4 \pm 1.9$  MPa and  $145.7 \pm 14.1\%$ , respectively. For the outer layer made of PLCL/COL-PDGF nanofiber yarns, the values were separately increased to  $17.5 \pm 2.0$  MPa and  $198.9 \pm 20.2\%$  at the tensile direction parallel to the alignment of the fiber yarns, mainly due to variation from single nanofiber to bonded fiber bundles. When moving the tensile from parallel to the perpendicular direction, the ultimate mechanical strength and elongation at break were changed to  $1.6 \pm 0.3$  MPa and  $208.6 \pm 18.7\%$ . For the vascular scaffold composed of the two layers, the values were  $14.9 \pm 2.4$  MPa and  $219.6 \pm 17.8\%$  for the parallel direction and  $3.7 \pm 0.6$  MPa and  $302.3 \pm 11.1\%$  for the perpendicular direction, respectively. These values are greater relative to the case of a porcine coronary artery (2.6 MPa and 100%, respectively). We also observed that the stress-strain curve of the vascular scaffold at the perpendicular direction had a long period with the stress close to 0. During this stage, we observed that only a very small number of stretched fibers were not completely broke until the stress was decreased to 0. As most of the nanofiber yarns in the outer layer were arranged with alignment in the parallel direction, the mechanical strength at the perpendicular direction was very low (Fig. 1G). When integrated with a layer of random nanofibers, a larger concentrated stress was needed to snap the bilayer scaffold at the perpendicular direction



**Fig. 2.** Cumulative release profiles of (A) heparin and (B) VEGF versus PDGF from the vascular scaffold post incubation in the PBS solution on a horizontal shaker at 37 °C and 120 rpm over a period of 45 days. (C) EPCs proliferation on the different types of nanofibers after culturing for 7 days. (D) SMCs proliferation on the different types of nanofibers and nanofiber yarns after culturing for 7 days. \* indicates significant difference between the compared groups at  $P < 0.05$  level.



**Fig. 3.** (A) SEM images and (B) fluorescence micrographs showing the morphology of EPCs after culturing on the inner layer (PLCL/COL-Hep/VEGF) of the vascular scaffold for 4 days. The PLCL/COL and PLCL/COL-Hep nanofibers were used as the control groups. (C) Fluorescence micrographs showing the morphology of SMCs after culturing on the outer layer (PLCL/COL-PDGF nanofiber yarns, NFY-P) for 4 days, together with the PLCL/COL nanofibers (NF), PLCL/COL-PDGF nanofibers (NF-P), and PLCL/COL nanofiber yarns (NFY) as the control groups. The actin cytoskeleton was stained with Alexa Fluor 555 phalloidin (red) in (B) and (C). (D) H&E staining showing the infiltration of SMCs into the NF-P and NFY-P samples after culturing for 4 days. (For interpretation of the references to colour in this figure legend, the reader is referred to the web version of this article.)

relative to the individual nanofiber yarn layer. However, the remained weak bonding between the adjacent nanofibers in the bundles could also resist the stretching under a low stress due to the extensive elongation of PLCL/COL fibers. As such, a protracted region with a low stress

near 0 was observed for the vascular scaffold at the perpendicular direction.

We have also measured that the compliance of the vascular scaffold was  $1.33 \pm 0.05\%/100 \text{ mmHg}$ . This value is comparable to that of human

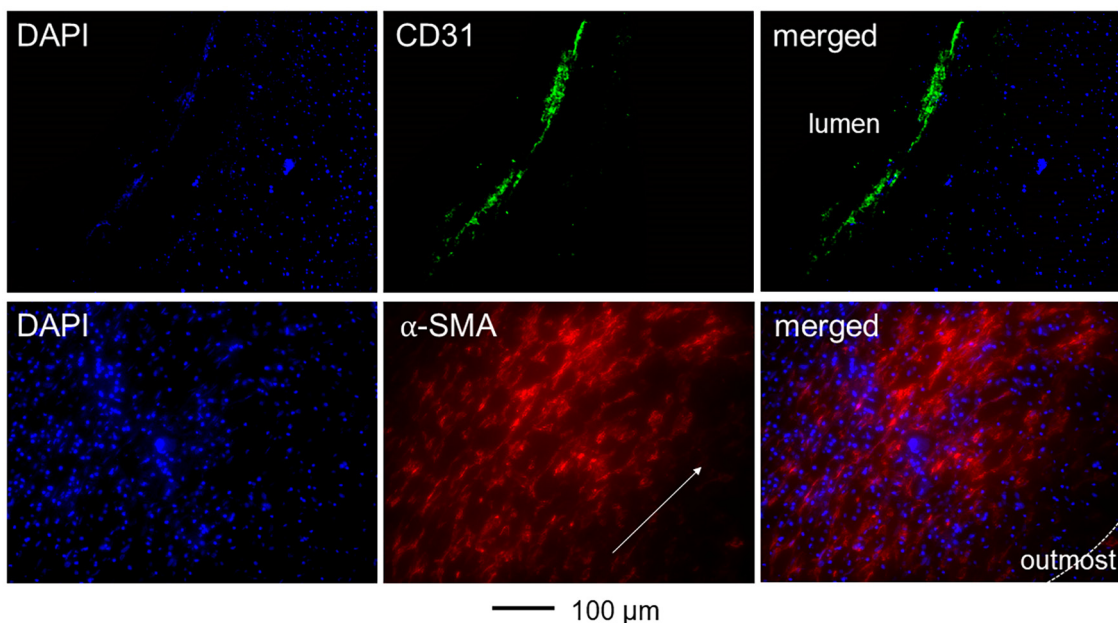


**Fig. 4.** Fluorescence micrographs of the vascular scaffold post immunohistochemical staining of DAPI, CD31, and  $\alpha$ -SMA after implantation for 2 months in a rat abdominal aortic defect model.

saphenous vein (0.7–1.5%/100 mmHg) and much better than that of the commercial e-PTFE graft (0.1%/100 mmHg, Table 2) [23,25]. It has been documented that the mechanical strength of a biodegradable vascular scaffold could be dramatically decreased with its degradation [26]. With a higher initial mechanical strength, we believe this vascular scaffold could meet the mechanical support needed for *in-situ* repair process.

### 3.2. Controlled release of the payloads from the vascular scaffold

In terms of the release of the different payloads from the vascular scaffold, we aim to realize a spatiotemporally controlled release of Hep/VEGF and PDGF from the lumen and tube wall, respectively, of the vascular scaffold through the specific design of the bilayers. We expect the homogeneous release of Hep/VEGF to hold the lumen patency of the vascular scaffold in the early-to-mid phase, while the relatively slow release of PDGF in a gradient increasing from the outmost layer toward the interior to reconstruct the vascular wall through the induction of SMCs infiltration. As shown by the cumulative release profiles of the payloads in Fig. 2, A and B, heparin and VEGF were separately released by  $72.3 \pm 4.0\%$  and  $75.9 \pm 4.0\%$  from the vascular scaffold at 45-day post incubation. In comparison, the released amount of PDGF was  $61.7 \pm 2.7\%$ . At each time point, the released amount of PDGF was smaller than that of VEGF, mainly due to the distinctive structure of the inner layer versus the outer layer of the vascular scaffold. For the nanofibers in the inner layer, VEGF was homogeneously incorporated into each individual fiber. For the nanofiber yarns in the out layer, however, PDGF was only loaded in half of the nanofibers, and the PDGF-loaded nanofibers were twisted with bare nanofibers inside the yarns, contributing to the slower release of PDGF with reference to VEGF from the inner layer. It has demonstrated that the formation of endothelium was prerequisite rather than the remodeling of the vascular media when repairing or regenerating vascular tissues, as the endothelial layer could provide a non-thrombogenic interface and prevent occlusion [27]. In this regard, such vascular scaffold with controlled release of VEGF and PDGF should be capable of *in-situ* reconstructing the different layers of the vasculature.

### 3.3. Manipulation of the growth behavior of EPCs and SMCs

Through the incorporation of multiple biological effectors, we can manipulate the growth of both EPCs and SMCs during the repair of defect vascular tissues. We firstly investigated the proliferation of EPCs on the PLCL/COL-Hep/VEGF nanofibers, together with PLCL/COL-Hep and PLCL/COL nanofibers as the control groups. As shown in Fig. 2C, EPCs proliferated significantly better ( $P < 0.05$ ) on the PLCL/COL nanofibers incorporated with VEGF relative to the cases of the nanofibers loaded with heparin only or without any payload at 1, 4, and 7-day post cell culture. It has been reported that VEGF promotes EPCs differentiation and rapid reendothelialization during vascular repair, thus improving the hemocompatibility and lumen patency of the implanted scaffold [13,28]. We then evaluated the growth of SMCs on the PLCL/COL nanofiber yarns loaded with PDGF (NFY-P) relative to the cases involving the use of PLCL/COL nanofibers loaded with PDGF (NF-P), PLCL/COL nanofiber yarns (NFY), and PLCL/COL nanofibers (NF), respectively. Fig. 2D shows the proliferation of SMCs on the different types of scaffolds. The SMCs seeded on the NFY scaffold showed significantly better proliferation (at  $P < 0.05$  level) when compared with the NF counterpart, showing that scaffold microstructure could affect the SMCs growth even they were fabricated from the same materials. The proliferation of SMCs was further significantly enhanced by incorporating PDGF into the nanofiber yarns (NFY-P versus NFY,  $P < 0.05$  level), indicating the bioactive effect provided by the growth factors.

We also investigated the morphology of EPCs and SMCs after culturing on the different types of scaffolds for 4 days. As shown by the SEM and fluorescence micrographs in Fig. 3, A and B, the EPCs tend to be more interconnected and confluent on the PLCL/COL-Hep/VEGF nanofibers with reference to the cases of PLCL/COL-Hep and PLCL/COL nanofibers. For the SMCs cultured on the different samples, we found significant differences in terms of cell alignment and infiltration even they were fabricated from the same raw materials. The morphologies of SMCs were significantly influenced by the topographic cues coming from the supported scaffolds. For the NFY-P and NFY scaffolds, SMCs grew and stretched in an orientation along with the alignment of the underneath fiber bundles, regardless of whether PDGF was

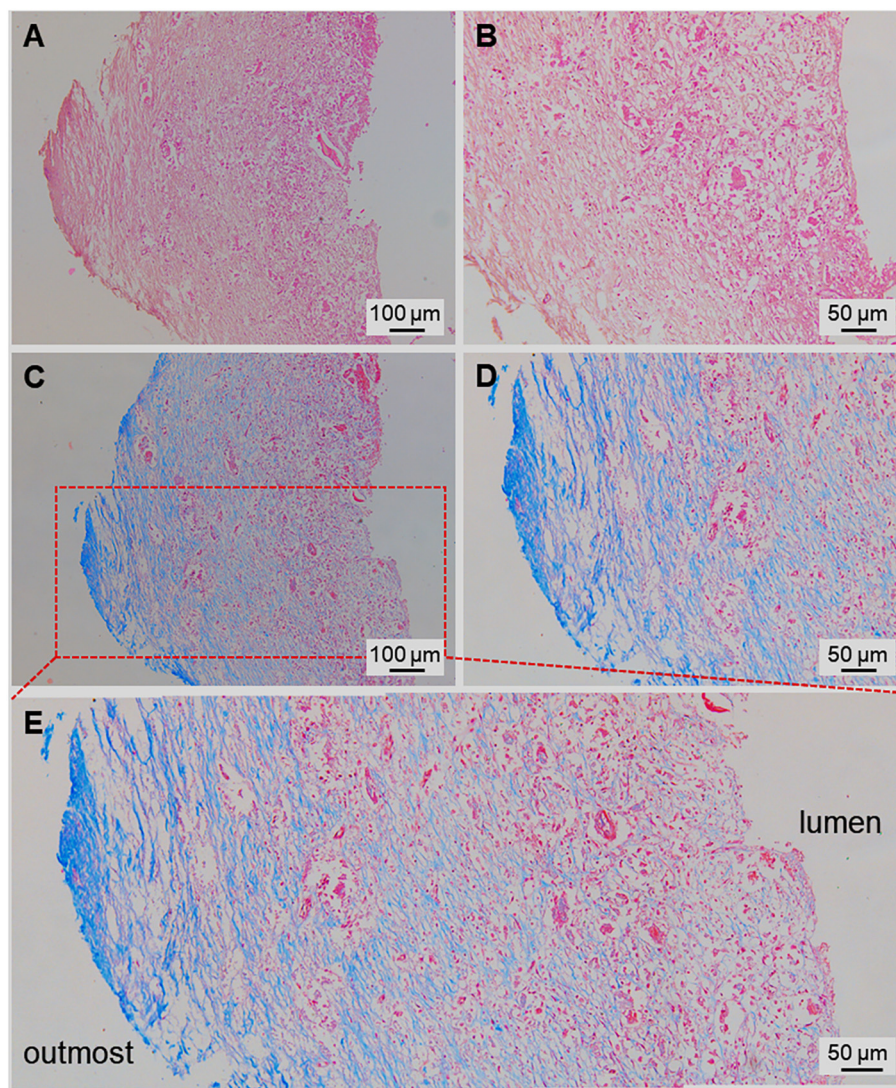


**Fig. 5.** Representative (A, B) H&E and (C – E) Masson's trichrome staining micrographs showing the cross section of the bilayer vascular scaffold after implantation in a rat abdominal aorta for two months. (E) The magnified micrograph of the rectangular area in (C).

incorporated (Fig. 3C). In comparison, the SMCs were randomly distributed with weak spreading on the NF-P and NF scaffolds. The uniaxially aligned nanofiber yarns encouraged the oriented growth and spreading of SMCs. From Fig. 3D, we showed that the SMCs could penetrate into the interior of the NFY-P scaffold only at 4-day post culturing, while the cells were only adhered on the surface of the NF-P sample. We also found that the infiltrated distance (*ca.* 18  $\mu\text{m}$ ) of cells for the NFY-P group was better than that (*ca.* 8  $\mu\text{m}$ ) of the NFY sample (Fig. S1). In these regards, we can conclude that both the porous structure provided by the nanofiber yarn structure and the biological guidance creating from the gradient PDGF contributed to the infiltration of SMCs toward the interior of the scaffold.

### 3.4. *In-situ* endothelialization and smooth muscle regeneration

We further investigated the *in-situ* endothelialization and infiltration of smooth muscle cells by implanting the vascular scaffold into the defect site of the abdominal aorta in a rat. At two-month post implantation, we found continuous endothelium on the lumen surface (CD31<sup>+</sup>, green) and oriented smooth muscles infiltrated into the vascular

wall ( $\alpha\text{-SMA}^+$ , red, Fig. 4 and Fig. S3). Such a structural distribution in terms of the endothelial cells and SMCs is consistent to the case of an autologous blood vessel (Fig. S2). Similar results were also obtained from the H&E and Masson's trichrome staining. As shown by the representative micrographs in Fig. 5, the macroscopical integrity of the blood vessel was well-maintained with the degradation of the scaffold and the regeneration of neotissues. The infiltration of cells was mainly reinforced by the valid spaces remained by scaffold degradation. As shown in Fig. 5, A and B, most of the scaffold materials were degraded with its fragments wrapped by cells and fibrous tissues. However, the exact percentage of the scaffold needs further investigation as it is highly relevant to the thickness of the two layers. From the current results, we have found that the thickness of regenerated tissues surrounding the vascular scaffold was greater than a native rat abdominal aorta (Fig. 5 and S4), indicating that the original thickness of the designed vascular scaffold should be decreased when used for repairing the rat abdominal aorta. To address this issue, we were able to precisely control the thickness of the nanofiber and nanofiber yarn layers as expected simply by tuning the collecting time. To suit use for different animal models including both small and large animals, we will further investigate the re-

relationship between the thickness of the different layers and the degradation rate, cell infiltration, and mechanical changes during the degradation in future studies.

In addition, a considerable number of muscle fibers (red) and collagen fibers (blue, Fig. 5, C and D) were produced in the interior and/or at the outmost of the vascular scaffold. Most particularly, the collagen fibers were produced in a gradation increasing from the interior of the scaffold toward the outside and achieved rich production at the outmost layer (Fig. 5E). Such collagen construction mimics the composition of a native vascular adventitia (Fig. S4), which is composed of thick and dense structures containing collagenous ECM [29,30]. Taken together, such kind of vascular scaffold holds great potential for *in-situ* endothelialization, smooth muscle alignment and infiltration, as well as collagen production when repairing injured blood vessels.

#### 4. Conclusion

In summary, we have demonstrated the design and fabrication of a vascular scaffold to facilitate *in-situ* rapid endothelialization and the orientation and infiltration of smooth muscle cells. The nanofibrous structure provided by the inner layer of the vascular scaffold mimicked the native structure of an extracellular matrix, contributing to the rapid formation of endothelium. The vascular wall was comprised of circumferentially aligned nanofiber yarns, which promoted the orientation and infiltration of SMCs. Owing to the different micro-structures of the two layers, we could realize the spatially uniform release of VEGF and graded release of PDGF, together with the difference in their release profiles to further promote rapid endothelialization in lumen and infiltration of smooth muscle cells toward the interior of the vascular wall. At two-month post implantation into a rat abdominal aorta, we showed the formation of a fluent endothelial layer at the luminal surface and infiltrated, aligned smooth muscles surrounding the vascular wall. A rich amount of collagen was also produced at the outmost layer of the vascular scaffold. Taken together, this vascular scaffold holds promising potential involving the repair or regeneration of defected vascular tissues.

#### Data availability

The raw/processed data required to reproduce these findings cannot be shared at this time as the data also forms part of an ongoing study. For private use only, please contact the authors.

#### Declaration of Competing Interest

The authors declare that they have no known competing financial interests or personal relationships that could have appeared to influence the work reported in this paper.

#### Acknowledgments

This research was supported by National Natural Science Foundation of China (31470941), Fundamental Research Funds for the Central Universities (CUSF-DH-D-2017047), and Qingdao Key Health Discipline Development Fund.

#### Appendix A. Supplementary data

Supplementary data to this article can be found online at <https://doi.org/10.1016/j.matdes.2021.109649>.

#### References

- [1] J. Liu, Y. Qin, Y. Wu, Z. Sun, B. Li, H. Jing, C. Zhang, C. Li, X. Leng, Z. Wang, D. Kong, The surrounding tissue contributes to smooth muscle cells' regeneration and vascularization of small diameter vascular grafts, *Biomater. Sci.* 7 (2019) 914–925.
- [2] S. De Valence, J.C. Tille, J.P. Giliberto, W. Mrowczynski, R. Gurny, B.H. Walpoth, M. Moller, Advantages of bilayered vascular grafts for surgical applicability and tissue regeneration, *Acta Biomater.* 8 (2012) 3914–3920.
- [3] S. Enomoto, M. Sumi, K. Kajimoto, Y. Nakazawa, R. Takahashi, C. Takabayashi, T. Asakura, M. Sata, Long-term patency of small-diameter vascular graft made from fibroin, a silk-based biodegradable material, *J. Vasc. Surg.* 51 (2010) 155–164.
- [4] D. Wang, X. Wang, X. Li, L. Jiang, Z. Chang, Q. Li, Biologically responsive, long-term release nanocoating on an electrospun scaffold for vascular endothelialization and anticoagulation, *Mater. Sci. Eng. C* 107 (2020) 110212.
- [5] J. Zhu, D. Chen, J. Du, X. Chen, J. Wang, H. Zhang, S. Chen, J. Wu, T. Zhu, X. Mo, Mechanical matching nanofibrous vascular scaffold with effective anticoagulation for vascular tissue engineering, *Compos. Part B* 186 (2020) 107788.
- [6] T. Wu, B. Jiang, Y. Wang, A. Yin, C. Huang, S. Wang, X. Mo, Electrospun poly(l-lactide-co-caprolactone)-collagen-chitosan vascular graft in a canine femoral artery model, *J. Mater. Chem. B* 3 (2015) 5760–5768.
- [7] T. Wu, J. Zhang, Y. Wang, B. Sun, M. Yin, G.L. Bowlin, X. Mo, Design and fabrication of a biomimetic vascular scaffold promoting *in situ* endothelialization and tunica media regeneration, *ACS Appl. Bio Mater.* 1 (2018) 833–844.
- [8] X. Jin, X. Geng, L. Jia, Z. Xu, L. Ye, Y. Gu, A.Y. Zhang, Z.G. Feng, Preparation of small-diameter tissue-engineered vascular grafts electrospun from heparin end-capped PCL and evaluation in a rabbit carotid artery replacement model, *Macromol. Biosci.* 19 (2019), e1900114.
- [9] L. West-Livingston, Y.M. Ju, H. Lee, R.L. Geary, A. Atala, S.J. Lee, Antibody-conjugated electrospun vascular scaffolds to enhance *in situ* endothelialization, *ACS Appl. Bio Mater.* 3 (2020) 4486–4494.
- [10] X. Ren, Y. Feng, J. Guo, H. Wang, Q. Li, J. Yang, X. Hao, J. Lv, N. Ma, W. Li, Surface modification and endothelialization of biomaterials as potential scaffolds for vascular tissue engineering applications, *Chem. Soc. Rev.* 44 (2015) 5680–5742.
- [11] Y. Duan, S. Yu, P. Xu, X. Wang, X. Feng, Z. Mao, C. Gao, Co-immobilization of CD133 antibodies, vascular endothelial growth factors, and REDV peptide promotes capture, proliferation, and differentiation of endothelial progenitor cells, *Acta Biomater.* 96 (2019) 137–148.
- [12] D. Wang, X. Wang, Z. Zhang, L. Wang, X. Li, Y. Xu, C. Ren, Q. Li, L.S. Turng, Programmed release of multimodal, cross-linked vascular endothelial growth factor and heparin layers on electrospun polycaprolactone vascular grafts, *ACS Appl. Mater. Interfaces* 11 (2019) 32533–32542.
- [13] L. Li, H. Liu, C. Xu, M. Deng, M. Song, X. Yu, S. Xu, X. Zhao, VEGF promotes endothelial progenitor cell differentiation and vascular repair through connexin 43, *Stem Cell Res Ther* 8 (2017) 237.
- [14] J. Shi, S. Chen, L. Wang, X. Zhang, J. Gao, L. Jiang, D. Tang, L. Zhang, A. Midgley, D. Kong, S. Wang, Rapid endothelialization and controlled smooth muscle regeneration by electrospun heparin-loaded polycaprolactone/gelatin hybrid vascular grafts, *J. Biomed. Mater. Res., B* 107 (2019) 2040–2049.
- [15] Z. Wang, Y. Wu, J. Wang, C. Zhang, H. Yan, M. Zhu, K. Wang, C. Li, Q. Xu, D. Kong, Effect of resveratrol on modulation of endothelial cells and macrophages for rapid vascular regeneration from electrospun poly(epsilon-caprolactone) scaffolds, *ACS Appl. Mater. Interfaces* 9 (2017) 19541–19551.
- [16] P. Zhou, F. Zhou, B. Liu, Y. Zhao, X. Yuan, Functional electrospun fibrous scaffolds with dextran-g-poly(l-lysine)-VAPG/microRNA-145 to specially modulate vascular SMCs, *J. Mater. Chem. B* 5 (2017) 9312–9325.
- [17] M. Wen, D. Zhi, L. Wang, C. Cui, Z. Huang, Y. Zhao, K. Wang, D. Kong, X. Yuan, Local delivery of dual microRNAs in trilayered electrospun grafts for vascular regeneration, *ACS Appl. Mater. Interfaces* 12 (2020) 6863–6875.
- [18] Y. Yang, D. Lei, H. Zou, S. Huang, Q. Yang, S. Li, F.-L. Qing, X. Ye, Z. You, Q. Zhao, Hybrid electrospun rapamycin-loaded small-diameter decellularized vascular grafts effectively inhibit intimal hyperplasia, *Acta Biomater.* 97 (2019) 321–332.
- [19] D. Wang, Y. Xu, Q. Li, L.S. Turng, Artificial small-diameter blood vessels: materials, fabrication, surface modification, mechanical properties, and bioactive functionalities, *J. Mater. Chem. B* 8 (2020) 1801–1822.
- [20] F. Han, X. Jia, D. Dai, X. Yang, J. Zhao, Y. Zhao, Y. Fan, X. Yuan, Performance of a multilayered small-diameter vascular scaffold dual-loaded with VEGF and PDGF, *Biomaterials* 34 (2013) 7302–7313.
- [21] S.G. Wise, M.J. Byrom, A. Waterhouse, P.G. Bannon, A.S. Weiss, M.K. Ng, A multilayered synthetic human elastin/polycaprolactone hybrid vascular graft with tailored mechanical properties, *Acta Biomater.* 7 (2011) 295–303.
- [22] Y.M. Ju, H. Ahn, J. Arenas-Herrera, C. Kim, M. Abolbashi, A. Atala, J.J. Yoo, S.J. Lee, Electrospun vascular scaffold for cellularized small diameter blood vessels: a pre-clinical large animal study, *Acta Biomater.* 59 (2017) 58–67.
- [23] A. Yin, C. Zhang, M.J. McClure, C. Huang, J. Wu, J. Fang, X. Mo, G.L. Bowlin, S.S. Al-Deyab, M. El-Newehy, Electrospinning collagen/chitosan/poly(L-lactic acid-co-caprolactone) to form a vascular graft: Mechanical and biological characterization, *J. Biomed. Mater. Res., A* 101A (2013) 1292–1301.
- [24] J. Yoon, H.S. Yang, B.S. Lee, W.R. Yu, Recent progress in coaxial electrospinning: new parameters, various structures, and wide applications, *Adv. Mater.* 30 (2018), e1704765.
- [25] N. L'Heureux, N. Dusserre, G. Konig, B. Victor, P. Keire, T.N. Wight, N.A.F. Chronos, A.E. Kyles, C.R. Gregory, G. Hoyt, R.C. Robbins, T.N. McAllister, Human tissue-engineered blood vessels for adult arterial revascularization, *Nat. Med.* 12 (2006) 361–365.

- [26] T. Wu, C. Huang, D. Li, A. Yin, W. Liu, J. Wang, J. Chen, H. Ei-Hamshary, S.S. Al-Deyab, X. Mo, A multi-layered vascular scaffold with symmetrical structure by bi-directional gradient electrospinning, *Colloids Surf. B* 133 (2015) 179–188.
- [27] W. Zheng, Z. Wang, L. Song, Q. Zhao, J. Zhang, D. Li, S. Wang, J. Han, X.L. Zheng, Z. Yang, D. Kong, Endothelialization and patency of RGD-functionalized vascular grafts in a rabbit carotid artery model, *Biomaterials* 33 (2012) 2880–2891.
- [28] W. Chen, L. Xiao, J. Bai, W. Zeng, M. Yang, B. Shi, C. Zhu, The promotion of tissue engineering blood vessel patency by CGS21680 through regulating pro-inflammatory activities of endothelial progenitor cell, *J. Biomed. Mater. Res., A* 106 (2018) 2634–2642.
- [29] I. Woods, A. Black, E.J. Molloy, S. Jockenhoevel, T.C. Flanagan, Fabrication of blood-derived elastogenic vascular grafts using electrospun fibrinogen and polycaprolactone composite scaffolds for paediatric applications, *J. Tissue Eng. Regen. Med.* 14 (2020) 1281–1295.
- [30] S. Cheng, Y. Jin, N. Wang, F. Cao, W. Zhang, W. Bai, W. Zheng, X. Jiang, Self-adjusting, polymeric multilayered roll that can keep the shapes of the blood vessel scaffolds during biodegradation, *Adv. Mater.* 29 (2017) 1700171.